MECHANICS

Biomechanics

Biological Flow in Large Vessels

Dialog Between Numerical Modeling and In Vitro/In Vivo Experiments

Coordinated by
Valérie Deplano
José-Maria Fullana
Claude Verdier

7

YALES2BIO: A General Purpose Solver Dedicated to Blood Flows

Simon MENDEZ[1], Alain BÉROD[1,2], Christophe CHNAFA[1,2], Morgane GARREAU[1,3], Etienne GIBAUD[1], Anthony LARROQUE[1], Stephanie LINDSEY[1], Marco MARTINS AFONSO[1], Pascal MATTÉOLI[1], Rodrigo MENDEZ ROJANO[1], Dorian MIDOU[1], Thomas PUISEUX[1,3], Julien SIGÜENZA[1,2], Pierre TARACONAT[1,4], Vladeta ZMIJANOVIC[1] and Franck NICOUD[1]

[1] *IMAG, CNRS, University of Montpellier, France*
[2] *Sim&Cure, Montpellier, France*
[3] *ALARA Expertise, Strasbourg, France*
[4] *Horiba Medical, Grabels, France*

Many cardiovascular diseases are related to blood flow features, and are able to predict how blood flows could open a door toward better diagnostic and treatment capabilities. To this respect, computational physics is complementary to theoretical, experimental and medical imaging techniques used to address questions related to either microscopic or macroscopic blood flows.

Many (medical) questions related to blood flows are relevant to the biggest arteries/veins of the cardiovascular system. The typical length scale ranges from 1 mm to a few centimeters and the typical Reynolds number can be as high as a few thousands. At these scales, blood is practically considered

For a color version of all the figures in this chapter, see www.iste.co.uk/deplano/biological.zip.

Biological Flow in Large Vessels,
coordinated by Valérie DEPLANO, José-Maria FULLANA, Claude VERDIER.

as a homogeneous fluid with either constant viscosity (typically $\mu = 3 \times 10^{-3}$ Pa.s) or characterized by a shear-thinning behavior. Typical issues that must be properly handled are then related to the highly complex and deformable geometry of the domain where blood flows, the transitional nature of the wall-bounded blood flow, the interaction with thin and highly deformable membranes (e.g. valve leaflets), thrombus formation due to the presence of biomedical materials and, of course, validation.

Blood is actually not homogeneous, but a dense (volume fraction in the range 20–50%) suspension of particles, ranging from 2 (platelets) to 20 μm (white blood cells) in size. More than 95% of the cells flowing in plasma are actually red blood cells, which are non-spherical (equivalent diameter 6 μm) particles. Because their reduced volume is only 0.65, red blood cells are highly deformable, their dynamics resulting from the coupling between the inner fluid (cytosol), the membrane of the cell and the outer fluid (plasma). In flow regimes typical of the micro-circulation, hemodynamics is dominated by suspension-related phenomena such as the non-inertial migration of red blood cells toward the center of the vessels.

This chapter describes some achievements and current modeling efforts based on the YALES2BIO solver (see: imag.umontpellier.fr/~yales2bio/) developed at IMAG (Montpellier, France). A short account about the numerical strategy is provided in section 7.1, where some validation test cases are also described. Examples of simulations performed to support modeling efforts are then provided in section 7.2, while section 7.3 gathers two industrial applications. Eventually, some on-going developments are described in section 7.4.

7.1. Methods and validation

YALES2BIO is a massively parallel multiphysics solver based on the YALES2 solver (see: www.coria-cfd.fr/index.php/YALES2) developed at CORIA (Rouen, France). YALES2BIO is dedicated to the simulation of blood flows at the macroscopic and microscopic scales. The base is a solver for the incompressible Navier–Stokes equations. The equations are discretized using a finite-volume fourth-order scheme, adapted to unstructured meshes (Moureau *et al.* 2011a,b). The divergence-free property of the velocity field is ensured thanks to the projection method introduced by Chorin (1968). The velocity field is first advanced in time using a low-storage fourth-order Runge–Kutta scheme (Moureau *et al.* 2011b, Chnafa *et al.* 2014) in a prediction step. This predicted field is then corrected by a pressure

gradient, obtained by solving a Poisson equation to calculate pressure. This equation is solved using the Deflated Preconditioned Conjugate Gradient algorithm (Malandain *et al.* 2013). For turbulence modeling, large-eddy simulations (LESs) are performed using the so-called sigma subgrid scale model (Nicoud *et al.* 2011), which guarantees that no eddy viscosity is applied for canonical laminar flows, and is well-suited to wall-bounded, as well as transitional flows (Nicoud *et al.* 2018). Computations may be performed with moving meshes, with an arbitrary Lagrangian–Eulerian formulation being used in such cases (Chnafa *et al.* 2014, 2016).

Several YALES2BIO simulations involve fluid-structure interaction, both at the macroscopic (Sigüenza *et al.* 2018) and microscopic scales (Lanotte *et al.* 2016, Mendez and Abkarian 2018). For fluid-structure coupling, YALES2BIO relies on Peskin's immersed boundary method (IBM) (Peskin 2002) for massless structures. The action of the structure is seen by the fluid as a force density applied in the prediction step. Forced Navier–Stokes equations are solved as described in the former paragraph. Once the flow velocity is calculated, the structure is simply convected by the flow, after the interpolation of the fluid velocity on the structure. The deformed structure being massless, it is always at equilibrium, which enables the calculation of forces at the nodes of the structure mesh. These forces are then regularized (or spread) over the fluid mesh. The original IBM, developed for Cartesian meshes has been adapted to unstructured meshes to comply with the data structure of YALES2BIO. This has been performed using the reproducing kernel particle method, which guarantees that the regularization and interpolation operators are coherent and reproduce a number of mathematical moments of the regularized/interpolated functions (Liu *et al.* 1995, Pinelli *et al.* 2010, Mendez *et al.* 2014). The cellular membrane mechanics are modeled by combining different models representing either the in-plane or out-of-plane resistances of the membrane (Skalak *et al.* 1973, Helfrich 1973). More details may be found in Mendez and Abkarian (2019). The method, originally developed for infinitely thin membranes, has also been extended to finite-size yet thin structures (Sigüenza *et al.* 2016, 2018). Numerous validation test cases have been presented in 2D (Mendez *et al.* 2014) and 3D (Sigüenza *et al.* 2016), in particular for the fluid–structure interaction coupling.

Our aim in confronting numerical results to reference data is not only to confirm the quality of the solver, but also to provide new understanding on the configuration. As an example, we developed new analytical solutions for the case of an inertial relaxation of a membrane immersed in fluid (Martins Afonso *et al.* 2014). Three other examples of advanced validation cases are

discussed in the remainder of this section to illustrate how simulating for validation may actually shed new light on the computed case itself.

7.1.1. *Food and Drug Administration case*

The configuration is the one proposed by the Food and Drug Administration (FDA) as a benchmark for computational fluid dynamics (CFD) in the context of biomedical engineering. It has been studied both experimentally and numerically by several independent research groups worldwide (Hariharan *et al.* 2011, Stewart *et al.* 2012). The geometry is axisymmetric with a long inlet section, a convergent nozzle, a throat section (10 diameters long) and a sudden expansion at the downstream end. The jet generated into the sudden expansion section may break down and become turbulent sooner or later depending on the flow regime. Five flow regimes were considered experimentally, ranging from fully laminar to fully turbulent and corresponding to $\mathrm{Re}_{th} = 500; 2000; 3500; 5000; 6500$ (Re_{th} is the Reynolds number based on the bulk velocity and throat diameter). From a turbulence modeling point of view, LES is better suited than the RANS approach to deal with flow situations at a moderate Reynolds number. It turns out that none of the 28 blinded, RANS-based CFD studies led to a good comparison with the FDA experimental results (Stewart *et al.* 2012), while more successful LES-based computations were achieved after the experimental results were released (Passerini *et al.* 2013, Delorme *et al.* 2013, Bhushan *et al.* 2013, Janiga 2014). This observation and the absence of sensitivity analysis in the successful, not-blinded studies question the actual predictive character of these simulations. YALES2BIO was thus used to address the robustness of the FDA simulation (Zmijanovic *et al.* 2017, Nicoud *et al.* 2018). The main outcome of this study is that a proper LES strategy can indeed reproduce the experimental results with good accuracy and for all of the flow regimes (from laminar to turbulent), as soon as small perturbations are superimposed to the inlet velocity profile. In the absence of inlet perturbations, the results are extremely sensitive (and thus neither robust nor predictive) to any numerical parameters, such as the numerical scheme, mesh topology and refinement or time step (see Figure 7.1 for an illustration). The necessity to inject perturbations at inlet in order to obtain robust and predictive simulations of the FDA configuration was recently demonstrated by another research group using a different numerical tool (Bergersen *et al.* 2019).

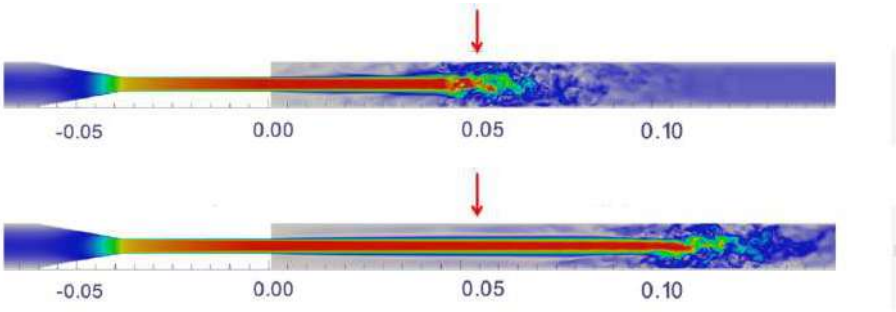

Figure 7.1. *Velocity map in the FDA nozzle showing the jet generated in the downstream pipe. The location of the jet breakdown (transition from laminar to turbulent) is well captured when a small time step is used (CFL = 0.1, top view), but not when a larger, yet numerically admissible, value is selected (CFL = 0.6, bottom view). The red arrow shows the position of the jet breakdown as observed in the experiment (Hariharan* et al. *2011)*

7.1.2. *Optical tweezers*

The validation of a solver dedicated to the dynamics of red blood cells (RBCs) is a challenge as it mixes physical complexity with biological complexity. In general, the validation includes fluid–structure interaction test cases with simpler particles such, as vesicles or spherical capsules (Yazdani *et al.* 2011, Barthès-Biesel 2009, 2016). It also relies on static cases in which the membrane mechanics alone are probed. This explains the success of the optical tweezers experiment (Dao *et al.* 2003, Mills *et al.* 2004) for validation (Li *et al.* 2005, Dao *et al.* 2006, Pivkin and Karniadakis 2008, Le *et al.* 2009, Fedosov *et al.* 2010a,b, Klöppel and Wall 2011, Chen and Boyle 2014, Farutin *et al.* 2014, Sinha and Graham 2015). In this configuration, two microbeads are attached on opposite sides of the RBC rim. One is fixed to a glass slide and the other one is controlled by a laser beam, which allows it to be displaced. The intensity of the laser beam allows the maximum force applied on the microbead to be fixed. The RBC is thus stretched by displacing the second beam with different forces. The sizes of the deformed RBC are measured in the direction of the stretching and in the normal direction, so that force-deformation curves can be obtained.

Simulations of a RBC stretched by optical tweezers have been performed using the YALESBIO solver (Sigüenza *et al.* 2017), with excellent comparisons with the experimental data from Mills *et al.* (2004). In addition, we clarified the meaning of this validation. It had been clearly shown that RBC simulations of the optical tweezers stretching are very sensitive to the

membrane shear modulus (Mills *et al.* 2004). However, the dependence to other deformation modes of the membrane was unclear. We first performed simulations with and without bending resistance (not shown) and changing the resistance to area stretching (see Figure 7.2(a)). We showed that results were rather insensitive to such parameters. As a result, this means that this validation test case can only assess the accuracy of the model representing the resistance to shear deformations of the membrane, and not the whole membrane model.

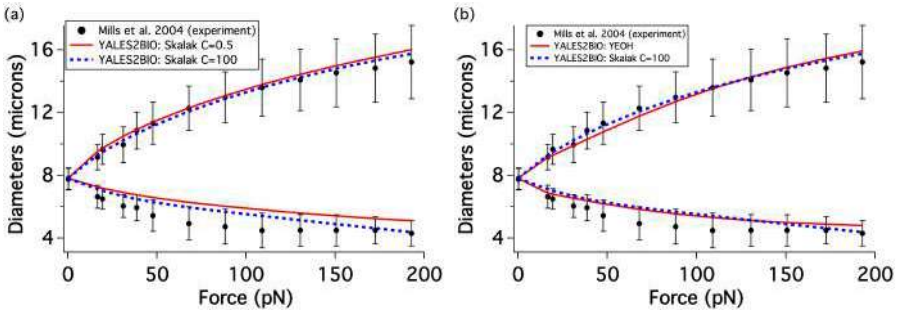

Figure 7.2. *Comparison of long and small diameters in the plane of view of an RBC stretched by optical tweezers, between simulations and experiments. a) Simulations with the same in-plane Skalak model using different values of C, the ratio between the area modulus and the shear modulus and b) simulations with the Skalak model with $C = 100$ and the Yeoh model (Mills* et al*. 2004)*

In addition, we showed that very different models could yield similar results, as shown in Figure 7.2(b), where results using either the Skalak model or the Yeoh model (see Mills *et al.* (2004), Sigüenza *et al.* (2017)) are compared. Both models align well. However, with the Yeoh model, the area of the RBC membrane increases by 30% (see Sigüenza *et al.* (2017)), which is impossible in RBCs. In addition, in order to obtain this fair comparison, the shear modulus of the Yeoh model has to be twice as large than that used with the Skalak model. The results presented by Sigüenza *et al.* (2017) thus show how cautious we have to be when using the optical tweezers for validation or assessment of the membrane mechanics. As detailed by Dimitrakopoulos (2012), this experiment focuses on large deformations of the cell. It is thus not a good configuration for assessing the shear modulus of the membrane, which is characteristic of small deformations: the value of the shear modulus inferred by the simulations depends on the model used. If the same membrane model is used, it is a good configuration to compare the resistance of different cells, but not the resistances to bending or area changes. Note, however, that the 3D shape of the RBC depends on such parameters, so that

more detailed 3D data from the experiment could yield a more thorough validation case for simulations (Sigüenza *et al.* 2017).

7.1.3. *Red blood cell self-organization*

The YALESBIO solver can also be run with multiple cells. The validation of this capability has been demonstrated by Iss *et al.* (2019), where the self-organization of RBCs in a rectangular channel has been computed. Iss *et al.* (2019) have shown that in microfluidic channels of height 9 μm and width 30 and 60 μm, RBCs self-organize in trains and lines at preferred distances from the lateral walls. Numerical simulations of RBC suspensions at different hematocrit values were performed in a periodic channel until convergence was reached in terms of structure, and compared to experimental images captured at the end of a 5-mm-long channel (see Figure 7.3). Simulations predict how RBCs organize in one, two or three files with increasing hematocrit well, as in the experiment. The essential role of deformability and lateral walls was also proved by numerical simulations. More details can be found in Iss *et al.* (2019).

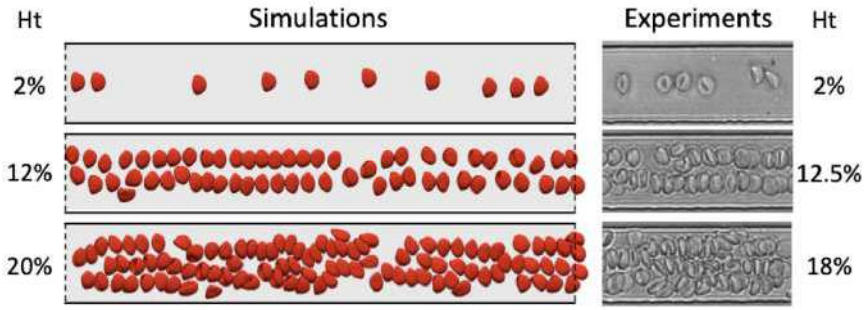

Figure 7.3. *Example of the structure of the flow in one, two or three lines for RBC suspensions at different hematocrits in a channel of height 9 μm (direction normal to the image) and width 30 μm (vertical direction). RBCs flow from left to right. Figure adapted from Iss* et al. *(2019)*

7.2. Simulation as support of modeling efforts

An interesting use of a flow solver is the generation of reference data as part of a modeling effort. With the increase in computing resources, more and more computationally demanding simulations become feasible, but the need for simplified models remains. In this context, numerical simulations may provide well-controlled data for building new low-order models to either

understand a particular phenomenon, account for some effect at a moderate cost in simulations or validate data reconstruction algorithms. This section provides some examples of the use of YALES2BIO simulations to support modeling.

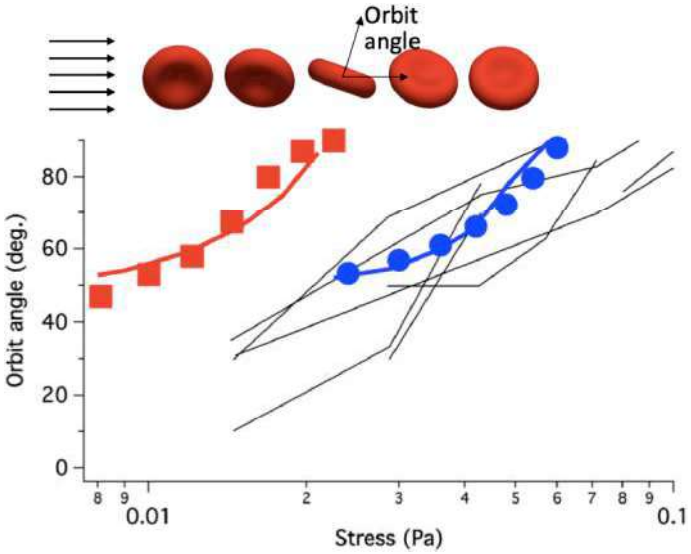

Figure 7.4. *Orbit angles of RBCs flipping under shear flow, as a function of the shear rate, at viscosity contrast 1.0. Black lines: experiments from Dupire* et al. *(2012). Symbols: YALES2BIO simulations for different stress-free shapes (red: quasi-sphere of reduced volume 0.997; blue: ellipsoid of reduced volume 0.96). Bold continuous lines: reduced-order model (Mendez and Abkarian 2018) changing the energy barrier to mimic the change of stress-free shape. The definition of the orbit angle is provided in the sequence of images extracted from a top view of the dynamics of a RBC flipping over an orbit*

7.2.1. *Single cell dynamics*

One fascinating aspect of the dynamics of red blood cells in shear flow (Mendez and Abkarian 2019) is their behavior at low shear stresses, for which RBCs exhibit very different motions without major deformations (Dupire *et al*. 2012). The absence of RBC deformations actually led to the consideration that their movement could be described by models developed for the motion of rigid objects, and in particular the model of Jeffery (1922), which predicts the motion of a rigid ellipsoid in shear flow. However, recent experiments have shown that contrary to rigidified RBCs, healthy RBCs flip

under shear over a specific orbit that depends on the shear rate. While the in-plane elasticity associated with the cytoskeleton was suspected to be a key element in the orbital selection and orbital drift, it was demonstrated for the first time by numerical simulations (Mendez and Abkarian 2018), by changing the stress-free shape of the cytoskeleton, which in turn controls the energy barrier that has to be overcome for the membrane to tank-tread (Abkarian *et al.* 2007). The effect is illustrated in Figure 7.4, which shows how the orbital drift (change of angle with shear rate) depends on the stress-free shape. This motivated the development of a low-order model reproducing all of the motions of RBCs at low shear rates (Mendez and Abkarian 2018). This model considers a fixed-shaped ellipsoid with a membrane that is able to tank-tread around it. By providing the appropriate modeling for the membrane elasticity, it displays all of the expected features of RBCs at low stresses, where deformation remains small: an example is the orbital drift predicted by such a model and displayed in Figure 7.4. This model opens the door to new theoretical developments in terms of RBC dynamics and blood flows.

7.2.2. *Flow diverters*

An intracranial aneurysm is an abnormal deformation of the arterial wall occurring in 3.6–6% of the general population, according to the systematic review by Rinkel *et al.* (1998). Since the prognosis[1] of subarachnoid hemorrhage is still very low, preventive surgery prior to rupture is considered as a therapeutic option by physicians (Hackenberg *et al.* 2018). Among all of the available treatments, flow-diverting type of devices are widely used due to their high rate of success (76%), low procedure-related morbidity (5%) and mortality (4%) (Brinjikji *et al.* 2013). The aim of these devices is to isolate the aneurysm from the parent artery blood flow, in order to promote a stable environment for thrombus formation (D'Urso *et al.* 2011). CFD has been extensively used to extract relevant indices that could discriminate successful and unsuccessful treatments (Ouared *et al.* 2016). To simulate the hemodynamic effect of a deployed flow-diverter inside patient-specific arterial geometries, two major techniques arise in the literature: *conformal* and *porous*. The first one subtracts the volume taken by the struts of the device from the arterial mesh. As struts are small compared to the size of the aneurysm, this leads to heavy computational costs. In order to reduce these costs, the porous method originally developed in Augsburger *et al.* (2010) uses a homogeneous approach by approximating the device as a porous

1 Predicting the likelihood of a person's survival.

material that imposes calibrated pressure losses through its surface via volumetric source terms added to the Navier–Stokes equations. Despite being computationally less expensive, the porous method requires an initial calibration and does not reproduce the effect of each strut on the flow. To circumvent these issues, a novel technique that is halfway between the conformal and porous methods has been developed and implemented in YALES2BIO (Alain *et al.* 2021). This framework has been compared to a "gold-standard" conformal computation of a steady flow through a patient-specific aneurysm. The results depicted in Figure 7.5 show that the implemented model compares reasonably well to the conformal results both locally near the wires and globally in the intra-aneurysmal recirculating region. The effort is currently geared toward validating this strategy using other conformal computations with different patient-specific and device geometries.

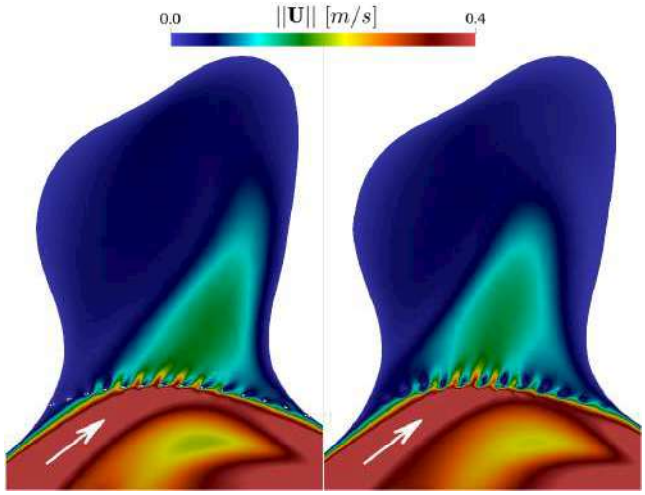

Figure 7.5. *Blood velocity magnitude in an aneurysm treated by a flow diverter, accounting for the device using a conformal approach (left) or a model (right). The white arrows show the mean flow direction*

7.2.3. *Echocardiography*

YALES2BIO was used to produce the intra-cardiac flow compatible with the time-evolving geometry observed from either the computed tomography of an actual patient (Chnafa *et al.* 2014) or magnetic resonance imaging of a normal volunteer (Chnafa *et al.* 2016). In both cases, the computational

domain extends from the four pulmonary veins to the root of the aorta and includes the left atrium and ventricles, as well as rough models of the mitral and aortic valves. The LESs were based on a subgrid scale model well suited to represent wall-bounded transitional flows (Nicoud *et al.* 2011) and performed over more than 50 cardiac cycles. The analysis revealed that turbulence is periodically generated in the left ventricle at the end of the diastole and washed out during systole (Chnafa *et al.* 2015). Moreover, the large vortex observed from advanced medical imaging techniques (Markl *et al.* 2011) at late diastole is well retrieved in the phase-averaged computational results. This flow feature is of particular interest from a medical point of view (it helps to redirect blood momentum toward the outlet of the ventricle and facilitates ejection) and being able to characterize it from routine echocardiography would be a useful feature for cardiologists. This requires being able to reconstruct the intra-ventricular velocity field from the knowledge of the radial component measured in color Doppler mode. The numerical database for the intraventricular flow (Chnafa *et al.* 2014) was used to support the development of a reconstruction algorithm based on an optimization procedure (Assi *et al.* 2017). As illustrated in Figure 7.6, the CFD recirculation zone is fairly well retrieved.

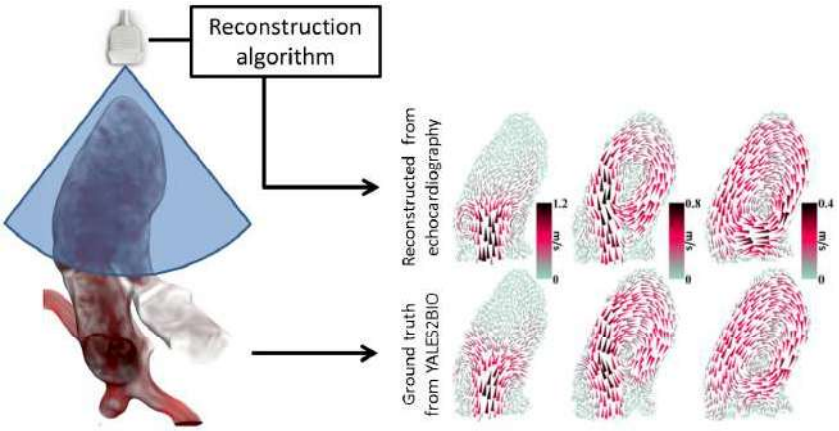

Figure 7.6. *Left: a virtual echocardiography exam is made on the numerical intra-cardiac flow. Right: the flow structure reconstructed from the virtual echocardiography image (top) is compared to the exact flow structure from the numerical database (bottom) at three different instants*

7.3. Simulations for industrial applications

7.3.1. *Flow in the Carmat artificial heart*

Since YALES2BIO relies on fully unstructured and parallelized numerical methods, it has the potential to tackle complex industrial configurations. A typical example is the total artificial heart developed by Carmat (see: www.carmatsa.com), which, from a fluid mechanics point of view, relies on the interaction between a biomimetic membrane and a working fluid operated by two rotating pumps to alternatively suck and push blood as an actual heart would do. Of course, the complexity of this blood-wetted device goes beyond the fluid–structure interaction problem, and ensuring the reliability of the control system and keeping the thrombogenic risk at a low level are other paramount issues to deal with when developing such a device. Still, handling the three elements (working oil, membrane, blood) fluid–structure problem in a complex geometry under pulsatile conditions is already quite challenging and was done using YALES2BIO (Larroque 2015). As an illustration, the membrane shape is shown at two instants in Figure 7.7. Note that the actual flow domain was truncated in this case (the casing where the two rotating pumps are located was not represented) and that the membrane dynamics were computed thanks to the LMGC90 software (Radjai and Dubois 2011) coupled with YALES2BIO, as detailed in Sigüenza *et al.* (2016). The ability of the YALES2BIO-LMGC90 coupling to handle macroscopic fluid–structure interaction problems accurately was demonstrated elsewhere (Sigüenza *et al.* 2016, 2018).

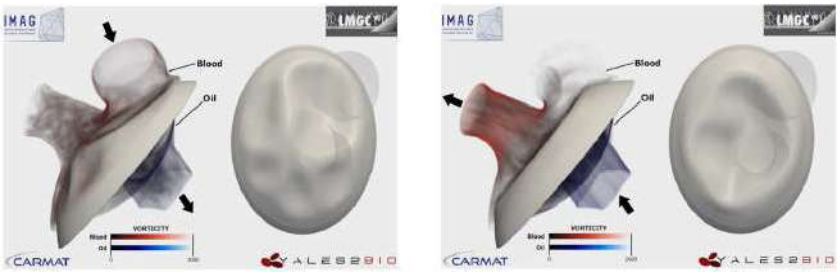

Figure 7.7. *3D view of the flow and membrane shape in a geometry inspired by the Carmat artificial heart during diastole (left) and systole (right). The black arrows show the mean flow direction. The red and blue color scales denote blood and oil (working fluid) vorticity renderings, respectively*

7.3.2. *Red blood cell dynamics in Horiba Medical's blood analyzers*

In a collaborative work between HORIBA Medical and IMAG, the impedance measurement of red blood cells in an industrial hematology analyzer was investigated (Taraconat *et al.* 2019). The configuration consists of a polarized micro-orifice in which RBCs are aspirated one at time. This constriction generates a high electrical field in the aperture so that the presence of the RBC induces an increase in electrical resistance that can be detected as voltage pulse. Numbering the electrical prints provides a count of cells that crossed the micro-orifice, and the amplitudes of the perturbations are assumed to be proportional to the particles size. Also known as the "Coulter counter" (Coulter 1953), this system thus yields measurements of the RBCs volumes and concentration. Coulter counters have been implemented in blood analyzers for decades, but some measurement artifacts are still misunderstood. In the neighborhood of the aperture walls, inhomogeneities of the electrical field and complex RBCs dynamics lead to measurement errors. Studying the dynamics of particles in the detection area to understand these edge-effects is an intricate task because industrial systems suffer from accessibility issues. This is why numerical simulation was preferred for investigations.

Handling the simulation of deforming cells in a Coulter counter involves a challenge that is multi-scale in nature, and has been overcome by a specific sequence of simulations, as proposed by Taraconat *et al.* (2019). The proposed method was compared with experimental measurements obtained from a healthy blood sample and a latex bead sample (see Figure 7.8). Numerical results not only reproduce the experimental observations, but also provide indications for the understanding of the complex signatures that arise when particles evolve in the wall vicinity. On the one hand, electrical edge-effects occur when particles encounter regions of highly heterogeneous electrical fields, near the aperture corner (see the blue circles in Figure 7.8). On the other hand, dynamical edge-effects consist of a cell rotation induced by substantial velocity shear located near the aperture walls (see the black arrows in Figure 7.8). Both types of artifacts impact the electrical prints, but they may be stratified thanks to the simulations (Taraconat *et al.* 2021).

7.4. Current developments

Most of the current challenges involve multi-physics and/or multi-scale situations. Three examples are provided in this section: modeling developments for the prediction of thrombotic events, modeling of the

velocity measurement by 4D flow magnetic resonance imaging (MRI) and the extension of YALES2BIO to dense suspensions of RBCs.

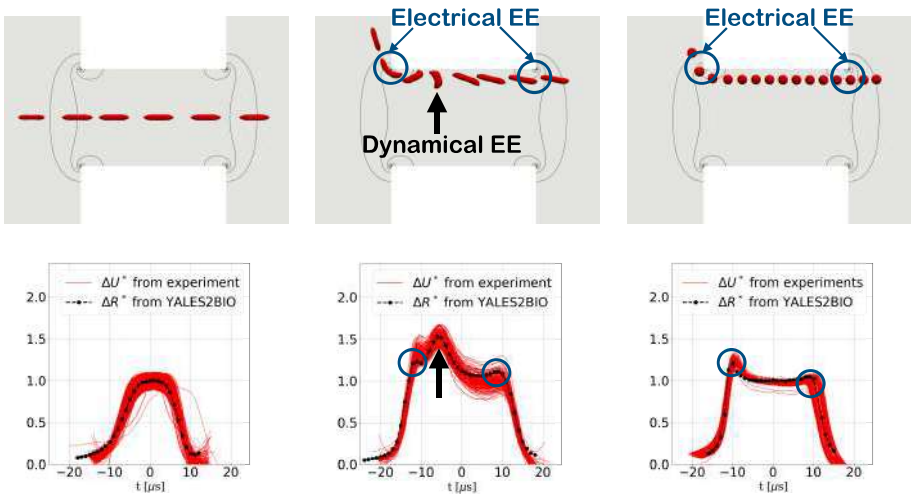

Figure 7.8. *The top row illustrates the simulated RBC dynamics in the micro-orifice, while the associated electrical perturbations are displayed in the bottom row. Electrical pulses arising from simulations are superimposed with experimental observations in the bottom row. The left, middle and right columns correspond to an RBC on a centered path, a RBC on a near-wall path and a rigid sphere on a near-wall path, respectively. Electrical field isolines are shown over the cut view of the fluid domain in the particle dynamics pictures in the top row. Electrical and dynamical edge-effects (EE) are highlighted by blue circles and black arrows, respectively*

7.4.1. *Thrombosis*

A major issue with blood-coated medical devices is their trend to produce extra blood coagulation (thrombosis) that may lead to device malfunction or thromboembolism (Manning *et al.* 2021). The adsorption/activation of the coagulation factor XII (Hageman factor) by the artificial surfaces of the devices is thought to be a key mechanism in this respect. A biochemical scheme (Chatterjee *et al.* 2010) was recently implemented in YALES2BIO to model thrombin generation by contact activation of factor XII with the device wall. To reflect mass conservation, a proper boundary condition was introduced that relates the species diffusive wall flux to the surface reaction rate of factor XII activation:

$$D\nabla_n[XII_a] + k_s[XII] = 0 \qquad [7.1]$$

In this equation, $[\cdot]$ is a molar fraction, ∇_n is the gradient operator along the direction normal to a solid boundary, XII_a is the activated form of factor XII, D stands for the species diffusivity in whole blood and k_s is a material property (surface reaction rate). This boundary condition contrasts with what is used in conventional in vivo models, in which the coagulation cascade is initiated at user-defined and arbitrary injury sites. This strategy was applied to a backward facing step geometry (Mendez Rojano *et al.* 2018) and a significant amount of thrombin was generated in the recirculation zone, as expected. Coupled to an existing model that represents platelet activity and thrombus growth (Taylor *et al.* 2016), the approach developed leads to a predictive pipeline for device-related thrombosis. This is illustrated in Figure 7.9, which shows that the generation of the thrombus is well captured, as well as its growth. Interestingly, this result was obtained without *a priori* knowledge of the regions prone to thrombosis: Equation 7.1 was prescribed in the same way everywhere and the appearance (or not) of a thrombus is controlled locally by the chemical-to-flow time scales ratio (a thrombus may only form if the fluid flow is slow enough to allow thrombin generation). Current research efforts are devoted to the reduction of the biochemical scheme (Chatterjee *et al.* 2010) used to predict thrombin formation (Mendez Rojano *et al.* 2019).

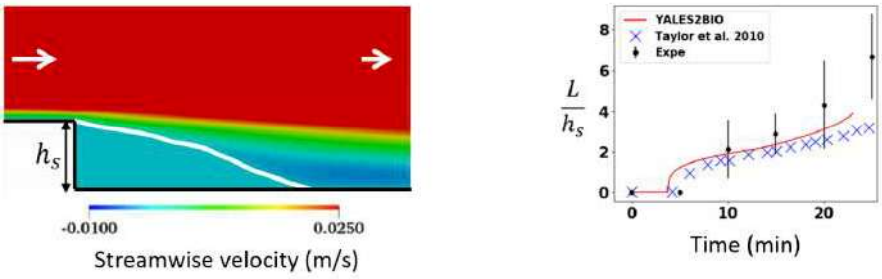

Figure 7.9. *Left: velocity map and boundary of the thrombus (thick white line). The white arrows show the mean flow direction. Right: time evolution of the length of the thrombus that appears behind the step, as observed in the experiment (Taylor* et al. *2014)*

7.4.2. *In Silico MRI*

Time-resolved 3D phase-contrast MRI (3D PCMRI, also called 4D flow MRI) is a promising tool for non-invasive blood flow quantification in vivo. As it relies on complex physical principles and the multi-modal acquisition

process, different types of velocity measurement errors arise, which might impair the diagnosis. A way to identify the origins of these measurement errors consists of numerically simulating the MRI experiment, governed by the Bloch equations (Bloch 1946), in order to reconstruct synthetic images that are exempt from experimental errors. However, the large variety of time scales generally induced by coupling the MRI equations to the flow motion, as well as the considerable acquisition times to simulate (of order 1000 s, say), results in prohibitive computational costs and largely contributs to making the simulations infeasible.

An Eulerian-Lagrangian 4D flow MRI simulation pipeline was developed, which benefits from the massively parallel capabilities of the YALES2BIO solver to solve the Bloch equations on Lagrangian particles with "on the fly" coupling to the CFD flow solver (Puiseux 2021). A semi-analytic formulation of the Bloch equations was proposed to accelerate the computations, and a specific particle injection strategy was implemented that uses the periodic removal of the transverse magnetization (RF-spoiling) to keep the particle distribution homogeneous and avoid zones of spurious signal. The coupling with the YALES2BIO solver was validated in several configurations (Puiseux 2021). A cardiovascular-like in vitro flow phantom was designed and integrated to a MRI-compatible experimental test bench (Puiseux *et al.* 2019). Several PC-MRI experiments were carried out and post-corrected from imaging artifacts. The compatible image-based CFD analysis was performed, prescribing the PC-MRI measurements as inlet velocity profiles. The CFD velocity field was downsampled to match the MRI spatiotemporal resolution, and compared to the experimental MRI velocity, resulting in 97% velocity correlations (Puiseux *et al.* 2019). Finally, coupled 4D flow MRI simulation was performed and the corresponding in silico velocity images were reconstructed and compared to the input CFD velocity field to validate the full simulation pipeline (see Figure 7.10). Both the experimental and simulated MRI velocity fields were compared with the downsampled CFD velocity field. As shown in Figure 7.10, the sites of largest velocity error seem well reproduced by the MRI simulation, although a systematically higher error is reported in the experimental MRI. We suggest that the large error site at the collateral-descending tube junction is a direct consequence of neglecting the acceleration in 4D flow MRI sequences. The remaining systematic error can be attributed to the experimental noise due to magnetic field inhomogeneities and off-resonance effects that are not accounted for in the MRI simulations.

7.4.3. *Multi-cells*

YALES2BIO is also extended to perform multi-cells simulations, as illustrated by the simulations of suspensions in microfluidic channels (Iss *et al*. 2019) already mentioned in the validation section. The aim is now to understand the relationship between single-cell behavior in shear flow, the motions of the cells in suspension and the macroscopic outcome, such as blood rheology, for instance. In particular, we have shown that RBCs in plasma subjected to increasing shear stress become more and more folded and compact (Mauer *et al*. 2018), which has beneficial effects on blood rheology, as demonstrated experimentally (Lanotte *et al*. 2016). Simulations may provide the explanation for this effect. In addition, our interpretation of blood dynamics is often driven by the knowledge on single cells. Systematic studies of the effect of increasing the concentration are still needed to determine to which extent single cell dynamics can be used to explain blood results. With this in mind, YALES2BIO now has the capability of performing multi-cells simulations, and computation in pure shear flow is currently being performed (see Figure 7.11) at various hematocrit levels.

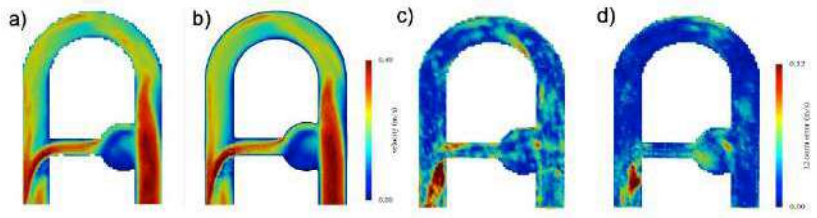

Figure 7.10. *Left: magnitude of the velocity a) reconstructed by MRI simulation and b) predicted by CFD at peak systole. Right: velocity L2-norm error reported for c) experimental MRI and d) simulated MRI, as compared to CFD*

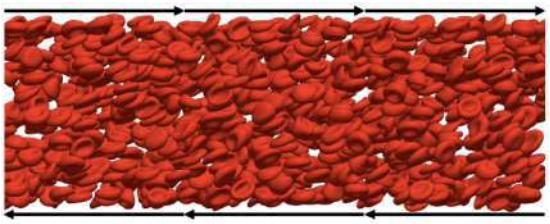

Figure 7.11. *RBC suspension under shear flow, at physiological viscosity contrast and shear rate 100 s^{-1}. Hematocrit is 12.5%*

7.5. Acknowledgments

The authors thank the ANR, the I-SITE Muse and the BPI for their support through the Laboratory of Excellence NUMEV (ANR-10-LABX-20), the FORCE (ANR-11-JS09-0011), the GLOBULE and the DAT@DIAG (ISI-I1112018W) projects. Dr. Moureau, Dr. Lartigue (CORIA, UMR 6614) and the SUCCESS scientific group are gratefully acknowledged for giving access to the YALES2 solver. This work was performed using HPC resources from GENCI-CINES (grants c2014037194 to c2016037194, A0020307194, A0040307194, and A0060307194) and from the platform MESO@LR.

7.6. References

Abkarian, M., Faivre, M., Viallat, A. (2007). Swinging of red blood cells under shear flow. *Physical Review Letters*, 98, 188302.

Alain, B., Chnafa, C., Mendez, S., Nicoud, F. (2021). A heterogeneous model of endovascular devices for the treatment of intracranial aneurysms. *International Journal for Numerical Methods in Biomedical Engineering* (in press) [Online]. Available at: https://doi.org/doi.org/10.1002/cnm.3552.

Assi, K., Gay, E., Chnafa, C., Mendez, S., Nicoud, F., Abascal, J., Lantelme, P., Tournoux, F., Garcia, D. (2017). Intraventricular vector flow mapping a Doppler-based regularized problem with automatic model selection. *Physics in Medicine & Biology*, 62(17), 7131–7147.

Augsburger, L., Reymond, P., Rufenacht, D.A., Stergiopulos, N. (2010). Intracranial stents being modeled as a porous medium: Flow simulation in stented cerebral aneurysms. *Annals of Biomedical Engineering*, 39(11), 850–863.

Barthès-Biesel, D. (2009). Capsule motion in flow: Deformation and membrane buckling. *Comptes rendus physique*, 10(8), 764–774.

Barthès-Biesel, D. (2016). Motion and deformation of elastic capsules and vesicles in flow. *Annual Review of Fluid Mechanics*, 48, 25–52.

Bergersen, A.W., Mortensen, M., Valen-Sendstad, K. (2019). The FDA nozzle benchmark: In theory there is no difference between theory and practice, but in practice there is. *International Journal for Numerical Methods in Biomedical Engineering*, 35(1), 1–10.

Bhushan, S., Walters, D., Burgreen, G. (2013). Laminar, turbulent, and transitional simulations in benchmark cases with cardiovascular device features. *Cardiovascular Engineering and Technology*, 4(4), 408–426.

Bloch, F. (1946). Nuclear induction. *Phys. Rev.*, 70(7–8), 460–474.

Brinjikji, W., Murad, M.H., Lanzino, G., Cloft, H.J., Kallmes, D.F. (2013). Endovascular treatment of intracranial aneurysms with flow diverters. *Stroke*, 44(2), 442–447.

Chatterjee, M.S., Denney, W.S., Jing, H., Diamond, S.L. (2010). Systems biology of coagulation initiation: Kinetics of thrombin generation in resting and activated human blood. *PLoS Computational Biology*, 6(9), e1000950.

Chen, M. and Boyle, F.J. (2014). Investigation of membrane mechanics using spring networks: Application to red-blood-cell modelling. *Materials Science and Engineering C*, 43, 506–516.

Chnafa, C., Mendez, S., Nicoud, F. (2014). Image-based large-eddy simulation in a realistic left heart. *Computers and Fluids*, 94, 173–187.

Chnafa, C., Mendez, S., Moreno, R., Nicoud, F. (2015). Using image-based CFD to investigate the intracardiac turbulence. In *Modeling the Heart and the Circulatory System. MS&A, Volume 14*, Quarteroni, A. (ed.). Springer International Publishing, New York.

Chnafa, C., Mendez, S., Nicoud, F. (2016). Image-based simulations show important flow fluctuations in a normal left ventricle: What could be the implications? *Annals of Biomedical Engineering*, 44(11), 3346–3358.

Chorin, A. (1968). Numerical solution of the Navier–Stokes equations. *Mathematics of Computation*, 22, 745–762.

Coulter, W.H. (1953). Means for counting particles suspended in a fluid. Patent #US2656508A.

Dao, M., Lim, C.T., Suresh, S. (2003). Mechanics of the human red blood cell deformed by optical tweezers. *Journal of the Mechanics and Physics of Solids*, 51, 2259–2280.

Dao, M., Li, J., Suresh, S. (2006). Molecularly based analysis of deformation of spectrin network and human erythrocyte. *Materials Science and Engineering C*, 26, 1232–1244.

Delorme, Y., Anupindi, K., Frankel, S. (2013). Large eddy simulation of FDA's idealized medical device. *Cardiovascular Engineering and Technology*, 4(4), 392–407.

Dimitrakopoulos, P. (2012). Analysis of the variation in the determination of the shear modulus of the erythrocyte membrane: Effects of the constitutive law and membrane modeling. *Physical Review E*, 85, 041917.

Dupire, J., Socol, M., Viallat, A. (2012). Full dynamics of a red blood cell in shear flow. *Proceedings of the National Academy of Sciences USA*, 109(51), 20808–20813.

D'Urso, P.I., Lanzino, G., Cloft, H.J., Kallmes, D.F. (2011). Flow diversion for intracranial aneurysms. *Stroke*, 42(8), 2363–2368.

Farutin, A., Biben, T., Misbah, C. (2014). 3D numerical simulations of vesicle and inextensible capsule dynamics. *Journal of Computational Physics*, 275, 539–568.

Fedosov, D.A., Caswell, B., Karniadakis, G. (2010a). Systematic coarse-graining of spectrin-level red blood cell models. *Computer Methods in Applied Mechanics and Engineering*, 199, 1937–1948.

Fedosov, D.A., Caswell, B., Karniadakis, G.E. (2010b). A multiscale red blood cell model with accurate mechanics, rheology, and dynamics. *Biophysical Journal*, 98, 2215–2225.

Hackenberg, K.A., Hänggi, D., Etminan, N. (2018). Unruptured intracranial aneurysms. *Stroke*, 49(9), 2268–2275.

Hariharan, P., Giarra, M., Reddy, V., Day, S., Manning, K., Deutsch, S., Stewart, S., Myers, M., Berman, M., Burgreen, G., Paterson, E., Malinauskas, R. (2011). Multilaboratory particle image velocimetry analysis of the FDA benchmark nozzle model to support validation of computational fluid dynamics simulations. *Journal of Biomechanical Engineering*, 133(4), 041002.

Helfrich, W. (1973). Elastic properties of lipid bilayers: Theory and possible experiments. *Z. Naturforsch*, 28, 693–703.

Iss, C., Midou, D., Moreau, A., Held, D., Charrier, A., Mendez, S., Viallat, A., Helfer, E. (2019). Self-organization of red blood cell suspensions under confined 2D flows. *Soft Matter*, 15, 2971–2980.

Janiga, G. (2014). Large eddy simulation of the FDA benchmark nozzle for a Reynolds number of 6500. *Computers in Biology and Medicine*, 47(April), 113–119.

Jeffery, G.B. (1922). The motion of ellipsoidal particles immersed in a viscous fluid. *Proceedings of the Royal Society of London, Series A*, 102(715), 161–179.

Klöppel, T. and Wall, W.A. (2011). A novel two-layer, coupled finite element approach for modeling the nonlinear elastic and viscoelastic behavior of human erythrocytes. *Biomechanics and Modeling in Mechanobiology*, 10, 445–459.

Lanotte, L., Mauer, J., Mendez, S., Fedosov, D.A., Fromental, J.-M., Claveria, V., Nicoud, F., Gompper, G., Abkarian, M. (2016). Red cells' dynamic morphologies govern blood shear thinning under microcirculatory flow conditions. *Proceedings of the National Academy of Sciences USA*, 113(47), 13289–13294.

Larroque, A. (2015). Haemodynamic simulations in a total artificial heart. Technical report, Université Paris-Sud & IMAG, Université de Montpellier.

Le, D.V., White, J., Peraire, J., Lim, K.M., Khoo, B.C. (2009). An implicit immersed boundary method for three-dimensional fluid-membrane interactions. *Journal of Computational Physics*, 228, 8427–8445.

Li, J., Dao, M., Lim, C.T., Suresh, S. (2005). Spectrin-level modeling of the cytoskeleton and optical tweezers stretching of the erythrocyte. *Biophysical Journal*, 88, 3707–3719.

Liu, W.K., Jun, S., Zhang, Y.F. (1995). Reproducing kernel particle methods. *International Journal for Numerical Methods in Fluids*, 20, 1081–1106.

Malandain, M., Maheu, N., Moureau, V. (2013). Optimization of the deflated conjugate gradient algorithm for the solving of elliptic equations on massively parallel machines. *Journal of Computational Physics*, 238, 32–47.

Manning, K.B., Nicoud, F., Susan, M.S. (2021). Mathematical and computational modeling of device-induced thrombosis. *Current Opinion in Biomedical Engineering*, 20, 100349 [Online]. Available at: https://doi.org/10.1016/j.cobme.2021.100349.

Markl, M., Kilner, P.J., Ebbers, T. (2021). Comprehensive 4D velocity mapping of the heart and great vessels by cardiovascular magnetic resonance. *J. Cardiovasc. Magn. Reson.*, 13(1), 7.

Martins Afonso, M., Mendez, S., Nicoud, F. (2014). On the damped oscillations of an elastic quasi-circular membrane in a two-dimensional incompressible fluid. *Journal of Fluid Mechanics*, 746, 300–331.

Mauer, J., Mendez, S., Lanotte, L., Nicoud, F., Abkarian, M., Gompper, G., Fedosov, D.A. (2018). Flow-induced transitions of red blood cell shapes under shear. *Physical Review Letters*, 121, 118103.

Mendez, S. and Abkarian, M. (2018). In-plane elasticity controls the full dynamics of red blood cells in shear flow. *Physical Review Fluids*, 3, 101101(R).

Mendez, S. and Abkarian, M. (2019). Single red blood cell dynamics in shear flow and their role in hemorheology. In *Dynamics of Blood Cell Suspensions in Microflows*, Mendez, S., Abkarian, M. (eds). CRC Press, Boca Raton.

Mendez, S., Gibaud, E., Nicoud, F. (2014). An unstructured solver for simulations of deformable particles in flows at arbitrary Reynolds numbers. *Journal of Computational Physics*, 256, 465–483.

Mendez Rojano, R., Mendez, S., Nicoud, F. (2018). Introducing the pro-coagulant contact system in the numerical assessment of device-related thrombosis. *Biomechanics and Modeling in Mechanobiology*, 17(3), 815–826.

Mendez Rojano, R., Mendez, S., Lucor, D., Ranc, A., Giansily-Blaizot, M., Schved, J.-F., Nicoud, F. (2019). Biomechanics and modeling in mechanobiology kinetics of the coagulation cascade including the contact activation system: Sensitivity analysis and model reduction. *Biomechanics and Modeling in Mechanobiology*, 18(4), 1139–1153.

Mills, J.P., Qie, L., Dao, M., Lim, C.T., Suresh, S. (2004). Nonlinear elastic and viscoelastic deformation of the human red blood cell with optical tweezers. *Mechanics & Chemistry of Biosystems*, 1(3), 169–180.

Moureau, V., Domingo, P., Vervisch, L. (2011a). Design of a massively parallel CFD code for complex geometries. *Comptes rendus mécanique*, 339(2–3), 141–148.

Moureau, V., Domingo, P., Vervisch, L. (2011b). From large-eddy simulation to direct numerical simulation of a lean premixed swirl flame: Filtered laminar flame-PDF modelling. *Combustion and Flame*, 158, 1340–1357.

Nicoud, F., Baya Toda, H., Cabrit, O., Bose, S., Lee, J. (2011). Using singular values to build a subgrid-scale model for large eddy simulations. *Physics of Fluids*, 23(8), 085106.

Nicoud, F., Chnafa, C., Siguenza, J., Zmijanovic, V., Mendez, S. (2018). Large-eddy simulation of turbulence in cardiovascular flows. In *Biomedical Technology. Lecture Notes in Applied and Computational Mechanics, Volume 84*, Wriggers, P., Lenarz, T. (eds). Springer, Cham [Online]. Available at: https://doi.org/10.1007/978-3-319-59548-1_9.

Ouared, R., Larrabide, I., Brina, O., Bouillot, P., Erceg, G., Yilmaz, H., Lovblad, K.O., Mendes Pereira, V. (2016). Computational fluid dynamics analysis of flow reduction induced by flow-diverting stents in intracranial aneurysms: A patient-unspecific hemodynamics change perspective. *Journal of NeuroInterventional Surgery*, 8, 1288–1293.

Passerini, T., Quaini, A., Villa, U., Veneziani, A., Canic, S. (2013). Validation of an open source framework for the simulation of blood flow in rigid and deformable vessels, 29(11), 1192–1213.

Peskin, C.S. (2002). The immersed boundary method. *Acta Numerica*, 11, 479–517.

Pinelli, A., Naqavi, I.Z., Piomelli, U., Favier, J. (2010). Immersed-boundary methods for general finite-difference and finite-volume Navier–Stokes solvers. *Journal of Computational Physics*, 229, 9073–9091.

Pivkin, I.V. and Karniadakis, G.E. (2008). Accurate coarse-grained modeling of red blood cells. *Physical Review Letters*, 101, 118105.

Puiseux, T., Sewonu, A., Meyrignac, O., Rousseau, H., Nicoud, F., Mendez, S., Moreno, R. (2019). Reconciling PC-MRI and CFD: An in-vitro study. *NMR in Biomedicine*, 32(5), e4063 [Online]. Available at: https://hal.archives-ouvertes.fr/hal-01962356. [Accessed 12 February 2019].

Puiseux, T., Sewonu, A., Moreno, R., Mendez, S., Nicoud, F. (2021). Numerical simulation of time-resolved 3D phase-contrast magnetic resonance imaging. *PLoS ONE*, 16(3), e0248816 [Online]. Available at: https://doi.org/10.1371/journal.pone.0248816. [Accessed 12 February 2019].

Radjai, F. and Dubois, F. (2011). *Discrete Numerical Modeling of Granular Materials*. ISTE Ltd, London, and John Wiley and Sons, New York.

Rinkel, G.J.E., Djibuti, M., Algra, A., van Gijn, J. (1998). Prevalence and risk of rupture of intracranial aneurysms. *Stroke*, 29(1), 251–256.

Sigüenza, J., Mendez, S., Ambard, D., Dubois, F., Jourdan, F., Mozul, R., Nicoud, F. (2016). Validation of an immersed thick boundary method for simulating fluid-structure interactions of deformable membranes. *Journal of Computational Physics*, 322, 723–746.

Sigüenza, J., Mendez, S., Nicoud, F. (2017). How should the optical tweezers experiment be used to characterize the red blood cell membrane mechanics? *Biomechanics and Modeling in Mechanobiology*, 16(5), 1645–1657.

Sigüenza, J., Pott, D., Mendez, S., Sonntag, S., Kaufmann, T., Steinseifer, U., Nicoud, F. (2018). Fluid-structure interaction of a pulsatile flow with an aortic valve model: A combined experimental and numerical study. *International Journal for Numerical Methods in Biomedical Engineering*, 34(4), 1–19.

Sinha, K. and Graham, M.D. (2015). Dynamics of a single red blood cell in simple shear flow. *Physical Review E*, 92, 042710.

Skalak, R., Tozeren, A., Zarda, R.P., Chien, S. (1973). Strain energy function of red blood cell membranes. *Biophysical Journal*, 13, 245–264.

Stewart, S., Paterson, E., Burgreen, G., Hariharan, P., Giarra, M., Reddy, V., Day, S., Manning, K., Deutsch, S., Berman, M., Myers, M., Malinauskas, R., Berman, M., Malinauskas, R. (2012). Assessment of CFD performance in simulations of an idealized medical device: Results of FDA's first computational interlaboratory study. *Cardiovascular Engineering and Technology*, 3(2), 139–160.

Taraconat, P., Gineys, J.-P., Isèbe, D., Nicoud, F., Mendez, S. (2019). Numerical simulation of deformable particles in a Coulter counter. *International Journal for Numerical Methods in Biomedical Engineering* [Online]. Available at: https://onlinelibrary.wiley.com/doi/10.1002/cnm.3243. [Accessed 2 August 2019].

Taraconat, P., Gineys, J.-P., Isèbe, S., Nicoud, F., Mendez, S. (2021). Detecting cells rotations for increasing the robustness of cell sizing by impedance measurements, with or without machine learning. *Cytometry*, 99(10), 977–86 [Online]. Available at: https://doi.org/10.1002/cyto.a.24356.

Taylor, J.O., Witmer, K.P., Neuberger, T., Craven, B.A., Meyer, R.S., Deutsch, S., Manning, K.B. (2014). In vitro quantification of time dependent thrombus size using magnetic resonance imaging and computational simulations of thrombus surface shear stresses. *Journal of Biomechanical Engineering*, 136(7), 1–11.

Taylor, J.O., Meyer, R.S., Deutsch, S., Manning, K.B. (2016). Development of a computational model for macroscopic predictions of device-induced thrombosis. *Biomechanics and Modeling in Mechanobiology* [Online]. Available at: http://link.springer.com/10.1007/s10237-016-0793-2.

Yazdani, A.Z.K., Kalluri, R.M., Bagchi, P. (2011). Tank-treading and tumbling frequencies of capsules and red blood cells. *Physical Review E*, 83, 046305.

Zmijanovic, V., Mendez, S., Moureau, V., Nicoud, F. (2017). About the numerical robustness of biomedical benchmark cases: Interlaboratory FDA's idealized medical device. *International Journal for Numerical Methods in Biomedical Engineering*, 33(1), 1–17 e02789.